Polymer Chemistry

Accepted Manuscript

ROYAL SOCIETY OF CHEMISTRY

www.rsc.org/polymers

ARTICLE TYPE www.rsc.org/xxxxxx | XXXXXXXX

Bifunctional Polybenzoxazine Nanocomposites Containing Photo-Crosslinkable Coumarin Units and Pyrene Units Capable of Dispersing Single-Walled Carbon Nanotubes

Mohamed Gamal Mohamed, Kuo-Chih Hsu, and Shiao-Wei Kuo*

Received (in XXX, XXX) Xth XXXXXXXXX 200X, Accepted Xth XXXXXXXXX 200X
First published on the web Xth XXXXXXXXX 200X
DOI: 10.1039/b000000x

In this study, we synthesized a new bifunctional benzoxazine monomer (Coumarin-Py BZ) possessing both coumarin and pyrene groups through the reaction of 4-methyl-7-hydroxycoumarin (Coumarin-OH), paraformaldehyde, and amino-pyrene (Py-NH_2) in 1,4-dioxane. Fourier transform infrared (FTIR) and ^1H and ^{13}C nuclear magnetic resonance spectroscopy confirmed the structure of this new Coumarin-Py BZ monomer. We used differential scanning calorimetry (DSC), thermogravimetric analysis (TGA), and FTIR spectroscopy to monitor the curing behavior of Coumarin-Py BZ to form poly(Coumarin-Py BZ), both before and after photodimerization of the coumarin moiety. DSC profiles revealed that the glass transition temperature of poly(Di-Coumarin-Py BZ) was higher than that of its corresponding polymer (poly(Coumarin-Py BZ)), consistent with an increase in crosslinking density after UV irradiation. The pyrene moiety of Coumarin-Py BZ enhanced the dispersibility of single-walled carbon nanotubes (SWCNTs) in THF, leading to the formation of highly dispersible Coumarin-Py BZ/SWCNT nanocomposites stabilized through π-π stacking between the pyrene and SWCNT units, as detected through fluorescence emission spectroscopy. The combination of photo-crosslinkable coumarin groups and SWCNT nanohybrids enhanced the glass transition temperature, thermal stability, and char yield of the polybenzoxazine matrix, based on DSC and TGA analyses.

Introduction

Polybenzoxazines (PBZs) are intriguing phenolic-type thermosets that are interesting both academically and industrially because of their wide molecular design flexibility and excellent physical and mechanical properties relative to those of other thermosetting resins.[1,2] The unique properties of PBZs—high glass transition temperatures, stable and low dielectric constants, high dimensional stability, low flammability, and low surface free energies—make them attractive materials for use in many applications.[3–10] In addition, the syntheses of PBZs are simple and benign: they are formed through thermal ring opening of corresponding benzoxazines, without the need for any catalyst, and without the release of any dangerous volatile compounds.[11–13]

Benzoxazine monomers are typically prepared through Mannich condensations of phenolic aromatic derivatives, paraformaldehyde, and primary amines. The wide variety of potential starting materials (phenols, amines) offers flexibility in the molecular design of the benzoxazine monomers, with many different structures having been reported.[14,15] During the process of self-crosslinking polymerization, the benzoxazine monomers are converted into PBZs having three-dimensional network structures. Several procedures have appeared recently for the modification of PBZ resins displaying excellent thermal properties. For example, the introduction of allyl or alkynyl side groups into the benzoxazine monomer can lead to covalently cross-linked structures exhibiting improved thermal and mechanical properties.[16] Alternatively, blending with others polymers [e.g., thermoplastic poly(*N*-vinyl-2-pyrrolidione)[17] homopolymer or thermosetting epoxy resin] or inorganic materials [e.g., clay,[18] polyhedral oligomeric silsesquioxane (POSS),[19] or carbon nanotubes (CNTs)[20]] can modify the thermal and mechanical properties of thermosetting PBZ resins.

The adhesion surface properties of an inorganic reinforcing material and a polymer matrix are dependent on the interactions present at their interfaces. Yu et al. prepared PBZ-modified multiwalled carbon nanotubes (MWCNTs) after initial treatment of the MWCNTs with HNO_3 followed by toluene-2,4-diisocyanate to introduce OH, COOH, and N=C=O groups, with the surface COOH groups then catalyzing the opening of the benzoxazine rings.[20(d)] Nevertheless, these covalently functionalized MWCNTs exhibited poorer optical, electronic, and mechanical properties because the orbital hybridization of some of its carbon atoms changed from sp^2 to sp^3.[21]

Noncovalent approaches toward modifying CNTs—taking advantage of hydrogen bonds, host–guest interactions, metal–ligand coordination, electrostatic interactions, and hydrophobic effects—have attracted much interest in recent years because such materials can exhibit outstanding properties.[22] The modification of CNTs using noncovalent interactions does not destroy the electronic conjugation, thereby maintaining the electronic and mechanical properties while enhancing dispersibility.[23] Dumas et al. reported that π-stacking interactions between CNTs and P-pPDA (a *p*-phenylenediamine–based benzoxazine) led to the formation of a reinforced network displaying excellent thermal and mechanical properties, with enhanced dispersion of unreacted MWCNTs in P-pPDA.[20(g)] We have also proposed a pyrene-based benzoxazine precursor that forms PBZ/CNT nanocomposites stabilized through strong π–π interactions between the pyrene units and CNT surfaces.[21]

Coumarins, cinnamic acids, and cinnamic esters display promising behavior as compounds capable of undergoing photoinduced crosslinking.[24] Upon irradiation at wavelengths greater than 310 nm, a coumarin moiety will undergo dimerization through [2π + 2π] cycloaddition to afford a crosslinked network, while de-crosslinking will occur upon irradiation at wavelengths of less than 260 nm. Zhao et al.

Department of Materials and Optoelectronic Science, Center for Nanoscience and Nanotechnology, National Sun Yat-Sen University, Kaohsiung, 804, Taiwan.
E-mail: kuosw@faculty.nsysu.edu.tw

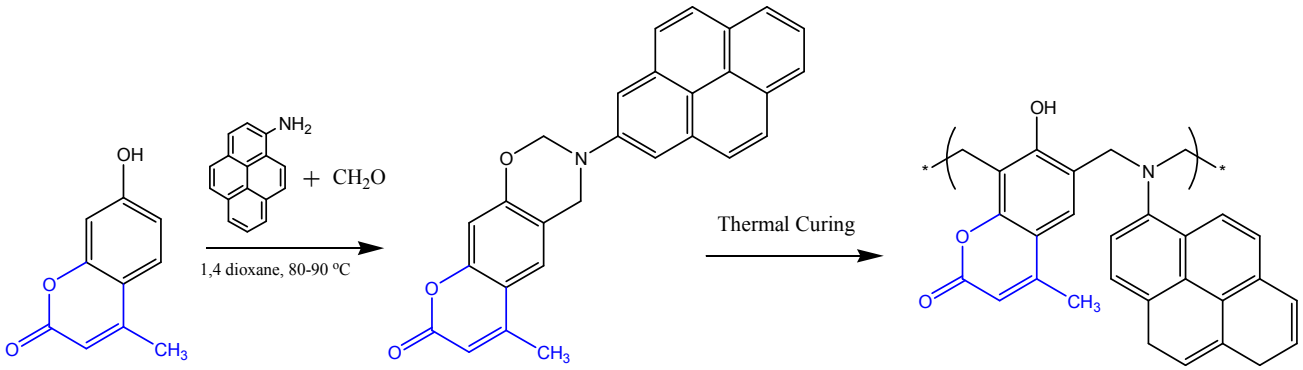

Scheme 1: Synthesis and chemical structures of Coumarin-Py BZ and poly(Coumarin-Py BZ).

incorporated coumarin derivatives in amphiphilic block copolymers and then used [2π + 2π] photocycloaddition of the coumarin groups under UV irradiation to fabricate a series of novel amphiphilic diblock copolymers featuring poly(ethylene oxide) blocks and various hydrophobic blocks, including poly(coumarin methacrylate) (PCMA), and random copolymers of poly(methyl methacrylate) (PMMA) and PCMA.[25] Yagci et al. were the first to incorporate a coumarin ring in a benzoxazine structure, which exhibited a high char yield after photodimerization of the coumarin units.[26]

In this study, we positioned both coumarin and pyrene bifunctional groups within a benzoxazine structure, obtaining the monomer Coumarin-Py BZ, which we then used to form high-performance PBZ/CNT nanocomposites, where photodimerization of the coumarin units enhanced the crosslinking density of the PBZ and the pyrene units enhanced the dispersion of CNTs within the polymer matrix through strong π–π interactions. Differential scanning calorimetry (DSC), Fourier transform infrared (FTIR) spectroscopy, and thermogravimetric analysis (TGA) revealed the thermal curing behavior and thermal stability of the benzoxazine monomer, both before and after photodimerization of the coumarin ring, and both in the presence and absence of the SWCNTs. In addition, we used UV–Vis and photoluminescence spectroscopy and transmission electron microscopy (TEM) to investigate the interactions and dispersion of the SWCNTs with the polymer after thermal curing.

Experimental Section

Materials

Paraformaldehyde (96%), pyrene, NaOH, and resorcinol were purchased from Acros. Ethyl acetoacetate was purchased from Showa. HNO_3 (65%), ACOH (99.8%), and H_2SO_4 (65%) were purchased from Scharlau. Hydrazine monohydrate (98%) was purchased from Alfa Aesar. $CHCl_3$, CH_2Cl_2, EtOH, tetrahydrofuran (THF), and 1,4-dioxane were purchased from Acros and used without further purification. 1-Nitropyrene was synthesized using a previously reported procedure.[21] SWCNTs were purchased from Center Biochemistry Technology.

Pyren-1-amine (Py-NH_2)

In a modified version of a procedure reported in the literature (Scheme S1),[21] 1-nitropyrene (10.0 g, 40.5 mmol) and 10% Pd/C (0.2 g) were dissolved/suspended in absolute EtOH (250 mL) and THF (150 mL) under N_2 in a 500-mL two-neck round-bottom flask equipped with a stirrer bar. The suspension was heated under reflux at 90 °C and then hydrazine monohydrate (15 mL) was added dropwise. After heating under reflux for a further 24 h, the mixture was cooled and filtered and then the filtrate was evaporated to dryness under reduced pressure. The crude product was recrystallized from cyclohexane and then further purified through column chromatography (n-hexane/THF, 4:1). Drying at 40 °C gave greenish yellow crystals (7.50 g, 85%); m.p.: 115–117 °C (DSC). FTIR (KBr, cm^{-1}): 3200-3400 (NH stretch). ^1H NMR (Figure S1, 500 MHz, DMSO-d_6, δ, ppm): 6.34 (s, 2H, NH_2), 7.34–8.28 (m, 9H, CCH). ^{13}C NMR (Figure S2, 125 MHz, DMSO-d_6, δ, ppm): 113.0 ($CHCHNH_2$), 121.1–132.9 (aromatic), 144.4 ($CHNH_2$).

4-Methyl-7-hydroxycoumarin (Coumarin-OH)

In a modified version of a procedure reported in the literature (Scheme S2),[26] concentrated H_2SO_4 (50 mL) was placed under a N_2 atmosphere in a 250-mL two-neck round-bottom flask equipped with a stirrer bar and cooled in an ice bath to 0 °C. A solution of resorcinol (5.00 g, 45.4 mmol) in ethyl acetoacetate (6.00 mL, 47.5 mmol) was added slowly with vigorous stirring to the flask, while maintaining the temperature below 5 °C. The mixture was stirred overnight at room temperature and then poured onto crashed ice with vigorous stirring. The solid that formed was filtered off under suction and washed with large amounts of cold water to remove any excess acid. The solid was extracted into CH_2Cl_2 (3 × 50 mL) and then the combined extracts were dried (anhydrous $MgSO_4$) for 30 min and concentrated under reduced pressure. The residue was recrystallized twice from MeOH to obtain white crystals (3.50 g, 85%); m.p. 188–190 °C (DSC). FTIR (KBr, cm^{-1}): 3137 (OH stretch), 1670 (C=O stretch). ^1H NMR (500 MHz, DMSO-d_6,δ, ppm): 2.40 (s, 3H, CH_3), 3.70 (s, 1H, OH), 6.08 (s, 1H, CH), 6.87 (d, 2H, CH), 7.45 (s, 1H, CH). ^{13}C NMR (125 MHz, $CDCl_3$,δ ppm): 18.3 (CH_3), 163.1 (C=O).

4-Methyl-7-(pyren-2-yl)-6,7-dihydrochromeno[6,7-*d*][1,2]oxazin-2(9*H*)-one (Coumarin-Py BZ)

A solution of 1-aminopyrene (1.00 g, 4.60 mmol) in 1,4-dioxane (25 mL) was added portionwise to a stirred solution of paraformaldehyde (0.290 g, 9.67 mmol) in 1,4-dioxane (50 mL) in a 150-mL three-neck round-bottom flask cooled in an ice bath. The mixture was then stirred for 30 min while maintaining the temperature below 5 °C. A solution of 4-methyl-7-hydroxycoumarin (0.810 g, 5.06 mmol) in 1,4-dioxane (30 mL) was added and then the mixture was heated under reflux while stirring for 12 h. After cooling the mixture to room temperature, the solvent was evaporated under reduced pressure to give a viscous oil, which was extracted into CH_2Cl_2 (3 × 80 mL); the combined extracts were washed several times with 1% NaOH and finally with distilled water. The organic phase was dried (anhydrous $MgSO_4$) for 1 h and then concentrated under pressure to afford a yellow solid, which was purified through column chromatography (SiO_2; *n*-hexane/EA, 1:1) to give a yellow solid

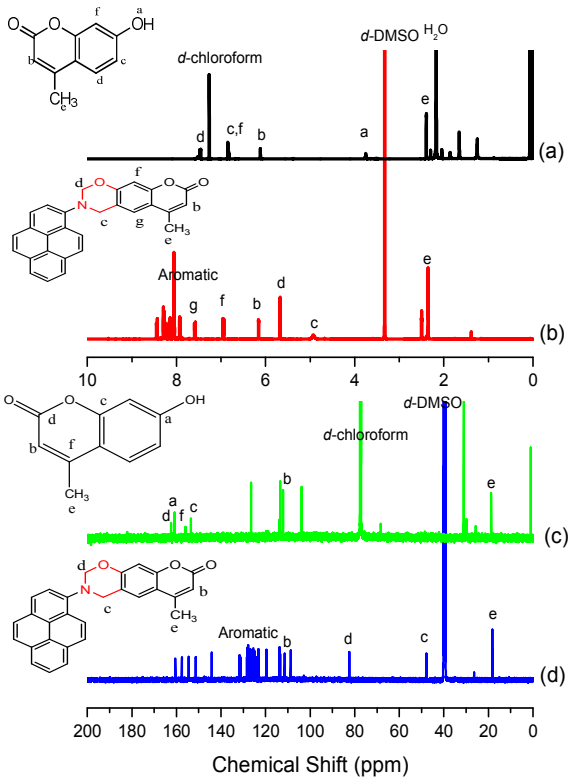

Figure 1: ^{1}H and ^{13}C NMR spectra of (a, c) Coumarin-OH and (b, d) Coumarin-Py BZ.

(1.40 g, 73%); m.p. 231 °C (DSC). FTIR (KBr, cm^{-1}): 1232 (asymmetric COC stretching), 1341 (CH_2 wagging), 931 and 1490 (vibration of trisubstituted benzene ring), 1730 (C=O stretching). ^{1}H NMR (500 MHz, $CDCl_3$,δ, ppm): 2.40 (s, 3H, **CH_3**), 4.84 (s, 2H, **CH_2**N), 5.59 (s, 2H, **OCH_2**N), 6.08 (s, 1H, **CH**), 6.94 (s, 2H), 6.92–8.43 (m, CH aromatic). ^{13}C NMR (125 MHz, DMSO-d_6, δ, ppm): 48.47 (**CCH_2N**), 80.04 (**OCH_2**N), 113.7–157.8 (aromatic), 160.5 (C=O).

Photodimerization of Coumarin-Py Benzoxazine

A solution of Coumarin-Py BZ (0.2 g) in $CHCl_3$ (10 mL) was placed in a quartz tube and irradiated for 15 min at room temperature in a merry-go-round–type photoreactor equipped with five Philips lamps emitting light nominally at 365 nm.

Coumarin-Py BZ/SWCNT Nanocomposites

Desired amounts of Coumarin-Py BZ (or Di-Coumarin-Py BZ) and SWCNTS were dissolved in THF through ultrasonication for 2 h. The mixture was stirred for 24 h at room temperature and then dried in a vacuum oven. Each nanocomposite was polymerized in a stepwise manner: at 110, 150, 180, and 210 °C for 2 h at each temperature The color of each cured sample was dark-red.

Characterization

^{1}H and ^{13}C nuclear magnetic resonance (NMR) spectra were recorded using an INOVA 500 instrument with DMSO-d_6 and $CDCl_3$ as solvents and tetramethylsilane as the external standard. Chemical shifts are reported in parts per million (ppm). FTIR spectra of the polymer films were recorded using a Bruker Tensor27 FTIR spectrophotometer and the conventional KBr disk method; 32 scans were collected at a spectral resolution of 4 cm^{-1}.

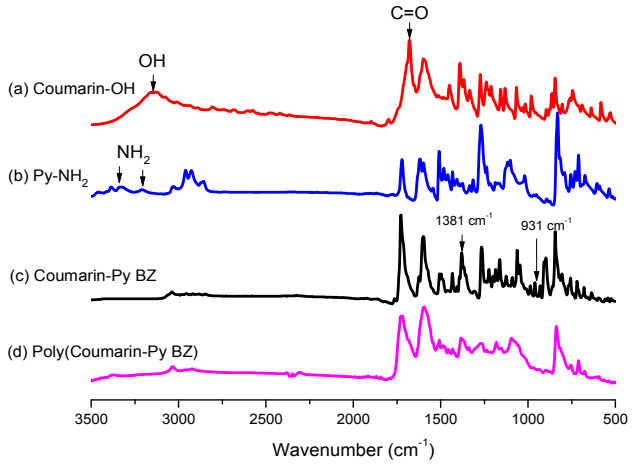

Figure 2: FTIR spectra of (a) Coumarin-OH, (b) Py-NH_2, (c) Coumarin-Py BZ, and (d) poly(Coumarin-Py BZ), recorded at room temperature.

The films tested in this study were sufficiently thin to obey the Beer–Lambert law. FTIR spectra recorded at elevated temperatures were obtained from a cell mounted inside the temperature-controlled compartment of the spectrometer. Dynamic curing kinetics were determined using a TA Q-20 differential scanning calorimeter operated under a N_2 atmosphere. The sample (ca. 5 mg) was placed in a sealed aluminum sample pan. Dynamic curing scans were recorded from 30 to 350 °C at a heating rate of 20 °C min^{-1}. The thermal stabilities of the samples were measured using a TA Q-50 thermogravimetric analyzer operated under a N_2 atmosphere. A cured sample (ca. 5 mg) was placed in a Pt cell and heated at a rate of 20 °C min^{-1} from 30 to 800 °C under a N_2 flow rate of 60 mL min^{-1}. UV–Vis spectra were recorded using a Shimadzu mini 1240 spectrophotometer; the concentration of Coumarin-Py BZ in THF was 10^{-4} M. Photodimerization of coumarin moieties was performed directly under a UV–Vis lamp at 365 nm (90 mW cm^{-1}). Photoluminescence (PL) excitation and emission spectra were collected at room temperature using a monochromatized Xe light source. TEM images were recorded using a JEOL-2100 transmission electron microscope operated at an accelerating voltage of 200 kV.

Results and Discussion

Preparation of Coumarin-Py BZ Monomer

We synthesized Coumarin-Py BZ through a three-step procedure. First, we prepared 1-aminopyrene through catalytic reduction of 1-nitropyrene over Pd/C. Next, we obtained 4-methyl-7-hydroxycoumarin through an acid-catalyzed reaction of resorcinol with ethyl acetoacetate. We then formed Coumarin-Py BZ through the reaction of Coumarin-OH, paraformaldehyde, and Py-NH_2 in 1,4-dioxane at 90–95 °C (Scheme 1). Figures 1(a) and 1(b) display the ^{1}H NMR spectra of Coumarin-OH and Coumarin-Py BZ, respectively. The spectrum of Coumarin-OH features signals at 2.40, 3.70, and 6.08 ppm corresponding to its CH_3, OH, and CH=C groups, respectively. The benzoxazine ring of Coumarin-Py BZ was characterized by signals at 4.93 (pyrene–CH_2N) and 5.64 (OCH_2N) ppm; no signal appeared for the NCH_2–pyrene unit near 4.00 ppm, suggesting that ring opening of the benzoxazine had not occurred and the signals for a pyrene moiety were present, confirming the synthesis of Coumarin-Py BZ. In addition, the areas about peaks ratio at 4.93 and 5.64 are close to 1:1 and thus our sample of Coumarin-Py BZ was of high

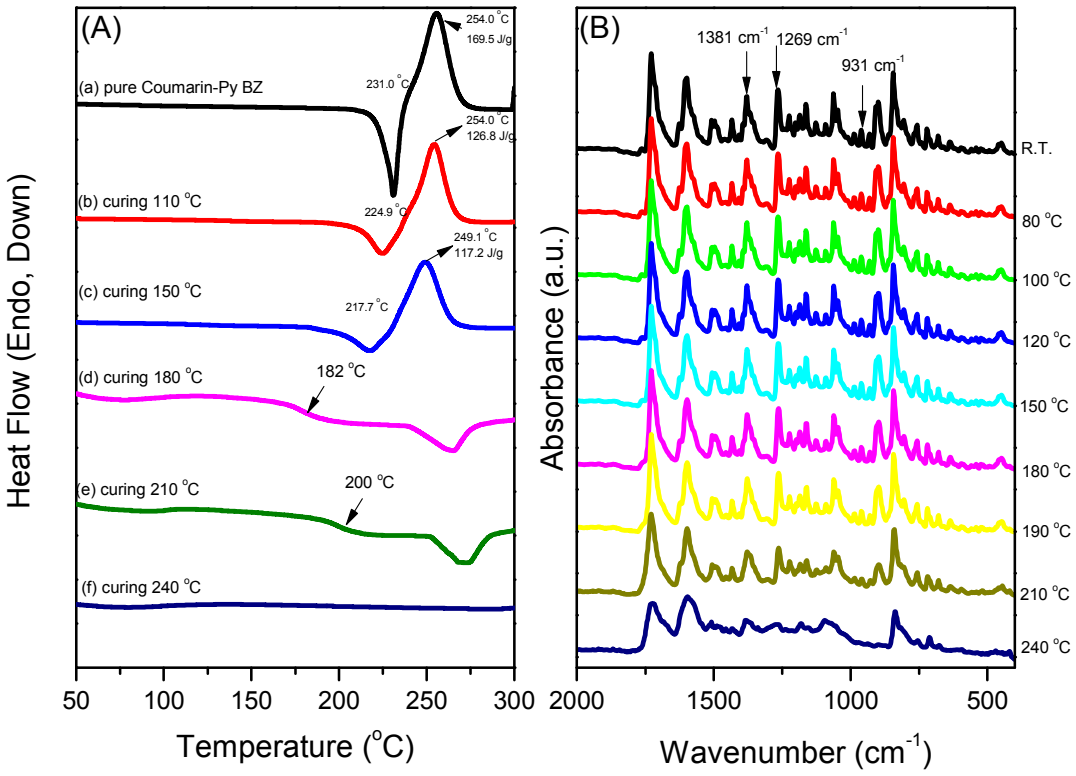

Figure 3: (A) DSC thermograms and (B) FTIR spectra of the Coumarin-PY BZ monomer, recorded after each heating stage.

purity. Figures 1(c) and 1(d) present the ^{13}C NMR spectra of Coumarin-OH and Coumarin-Py BZ, respectively. The characteristic peaks for the CH_3 and C=O groups of Coumarin-OH appeared at 18 and 163 ppm, respectively. In the spectrum of Coumarin-Py BZ, characteristic peaks appeared for the $PhCH_2N$ and OCH_2N units of the benzoxazine rings at 46.6, and 83 ppm, respectively, confirming the benzoxazine ring structure of Coumarin-Py BZ [Figure 1(d)]. Figure 2 presents the ambient-temperature FTIR spectra of Coumarin-OH, Py-NH_2, Coumarin-Py BZ, and, after thermal curing, poly(Coumarin-Py BZ). The spectrum of Coumarin-OH features a sharp signal for the OH group at 3200 cm^{-1} and a signal for the C=O group at 1677 cm^{-1} [Figure 2(a)]. The spectrum of Py-NH_2 reveals two sharp peaks for the amino group at 3200–3460 cm^{-1} and absorption bands for the pyrene unit at 831, 1599, 1619, and 3033 cm^{-1} [Figure 2(b)]. In the spectrum of Coumarin-Py BZ, the signals for the OH group of the coumarin moiety and the amino group of the pyrene ring were absent. In addition, we observed characteristic absorption peaks of a benzoxazine structure, for the 1,2,4-trisubstitued benzene rings (1490 and 931 cm^{-1}), and for asymmetric COC stretching (1232 cm^{-1}). The FTIR spectrum of Coumarin-Py BZ also featured characteristic absorption bands for its aromatic rings at 3033 (CH stretching), 1642 (C=C stretching), and 1730 (C=O stretching) cm^{-1} [Figure 2(c)]. Thus, the NMR and FTIR spectroscopic data confirmed the chemical structure and successful synthesis of Coumarin-Py BZ with high yield and purity. In addition, Figure 2(d) presents FTIR spectra of pure Coumarin-Py BZ after each curing cycle. The characteristic absorption bands of the trisubstituted aromatic ring of Coumarin-Py BZ (1490 and 931 cm^{-1}) disappeared after thermal curing; broad absorption bands appeared at 2500–3500 cm^{-1} in Figure 2(d), representing different kinds of hydrogen bonding interactions.[27]

Thermal Polymerization of Coumarin-Py BZ

We used FTIR spectroscopy and DSC to study the thermal polymerization of the coumarin/pyrene-based benzoxazine monomer, monitoring the changes in the characteristic peaks of the benzoxazine ring and the enthalpy of exotherms, respectively. Figure 3(A) presents DSC thermograms of Coumarin-Py BZ after each curing cycle, recorded at a heating rate of 20 °C min^{-1}. The DSC pattern of the uncured Coumarin-Py BZ featured a sharp melting point at 231.0 °C, and a maximum with an exothermic peak at 254.0 °C, and a reaction heat of 169.5 J g^{-1}. This curing temperature is lower than those of model pyrene-functionalized benzoxazines (Py-BZ) lacking a coumarin unit;[21] they generally exhibit exothermic ring opening at 286.0 °C, as displayed in Figure S3, suggesting that the coumarin moiety acted as a catalyst that contributed to the lower polymerization temperature. We can find that the enthalpy of exotherms decreased upon increasing the curing temperature of Coumarin-Py BZ. The exotherm peak disappeared completely after applying a curing temperature of only 240 °C, indicating that the curing reaction of the benzoxazine was complete at this temperature. Interestingly, the glass transition temperatures of the poly(Coumarin-Py BZ) products were higher—at 182 and 200 °C, respectively—after thermal curing at temperatures of 180 and 210 °C, respectively; thus, a higher curing temperature led to a higher glass transition temperature, as is generally observed in thermosetting systems. Figure 3(B) displays FTIR spectra of the Coumarin-Py BZ monomer and its products after each curing stage. The intensities of the characteristic absorption bands at 1234 (asymmetric COC stretching of oxazine), 1030 (symmetric COC stretching of oxazine), 1120 (CNC asymmetric stretching), 1322 (CH_2 wagging), 1496 (stretching of trisubstituted benzene ring), and 931 (CH out-of-plane bending) cm^{-1} gradually decreased upon increasing the curing temperature. When curing temperature

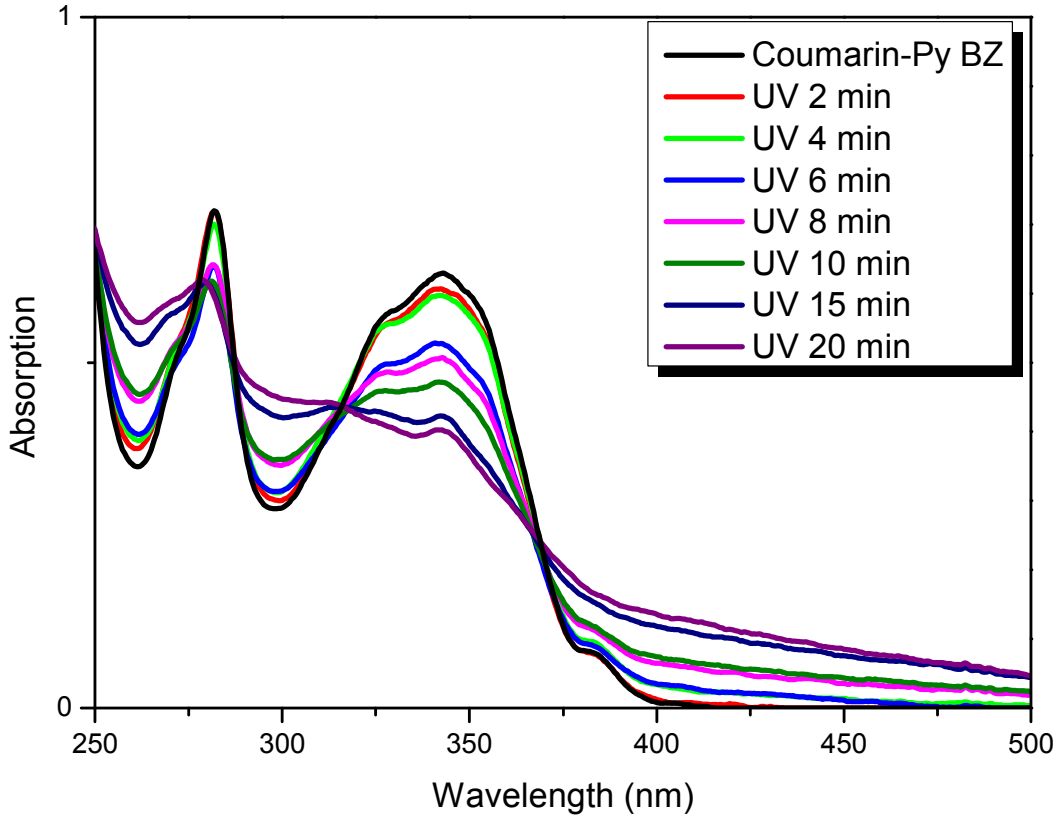

Figure 4: Changes in UV–Vis absorbance of Coumarin-Py BZ solutions in THF after irradiation at 365 nm.

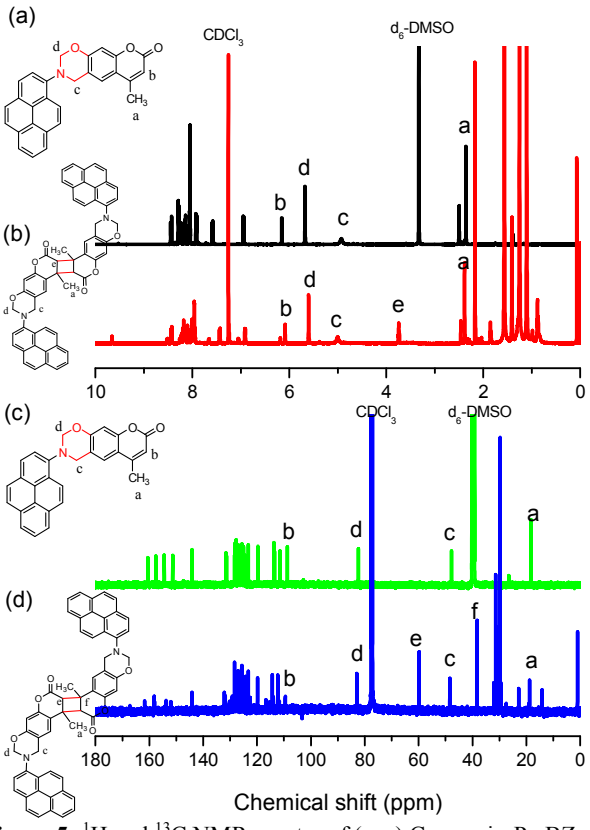

Figure 5: ^{1}H and ^{13}C NMR spectra of (a, c) Coumarin-Py BZ and (b, d) Di-Coumarin-Py BZ.

reached 240 °C, the characteristic absorption bands for the benzoxazine had disappeared completely, consistent with our results from the DSC analyses.

Photodimerization Through [2π–2π] Cycloaddition of Coumarin Moieties

The coumarin moiety undergoes photochemical dimerization through singlet and triplet excited states upon direct irradiation.[26] Upon UV irradiation at wavelengths above 300 nm, the absorption bands of coumarin derivatives appear between 250 and 300 nm, as a result of the π–π* transition of the conjugated aromatic nucleus, and between 310 and 345 nm, for the π–π* transition of the pyrone unit.[28] Figure 4 presents UV–Vis spectra of Coumarin-Py BZ after irradiation for various intervals of time; the trend in the decrease in the intensity of the absorption band near 343 nm time is consistent with [2π + 2π] dimerization of the olefinic bonds, thereby destroying the delocalized π system. We calculated the degree of dimerization of the 4-methylcoumarin moiety of Coumarin-Py BZ using the equation

$$\text{Degree of dimerization} = (1 - A_t/A_0) \times 100$$

where A_t and A_0 are the absorbances of the coumarin unit at 343 nm after irradiation times t and zero, respectively. The degree of dimerization for this system after irradiation for 20 min was approximately 63%. Figure 5 presents the ^{1}H and ^{13}C NMR spectra of Coumarin-Py BZ after photodimerization through [2π + 2π] cycloaddition of its coumarin ring (cf. Figure 1 for the corresponding spectra recorded before UV irradiation). UV irradiation at 365 nm for 15 min resulted in two new peaks appearing in the ^{1}H NMR spectrum at 3.7 and 1.4 ppm, representing the CH units of cyclobutane rings and CH_3 groups, respectively [Figure 5(b)]. The overall degree of dimerization, as determined through ^{1}H NMR spectroscopic analysis of the signal

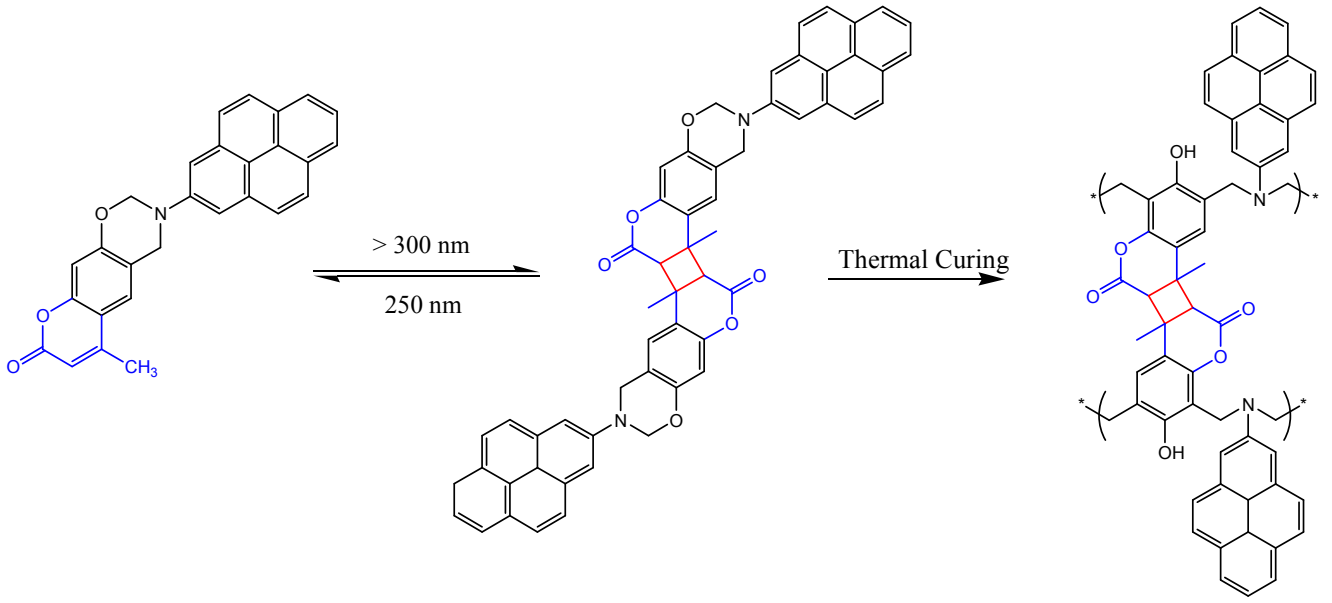

Scheme 2: Photodimerization of Coumarin-Py BZ and subsequent thermal curing to form poly(Di-Coumarin-Py BZ).

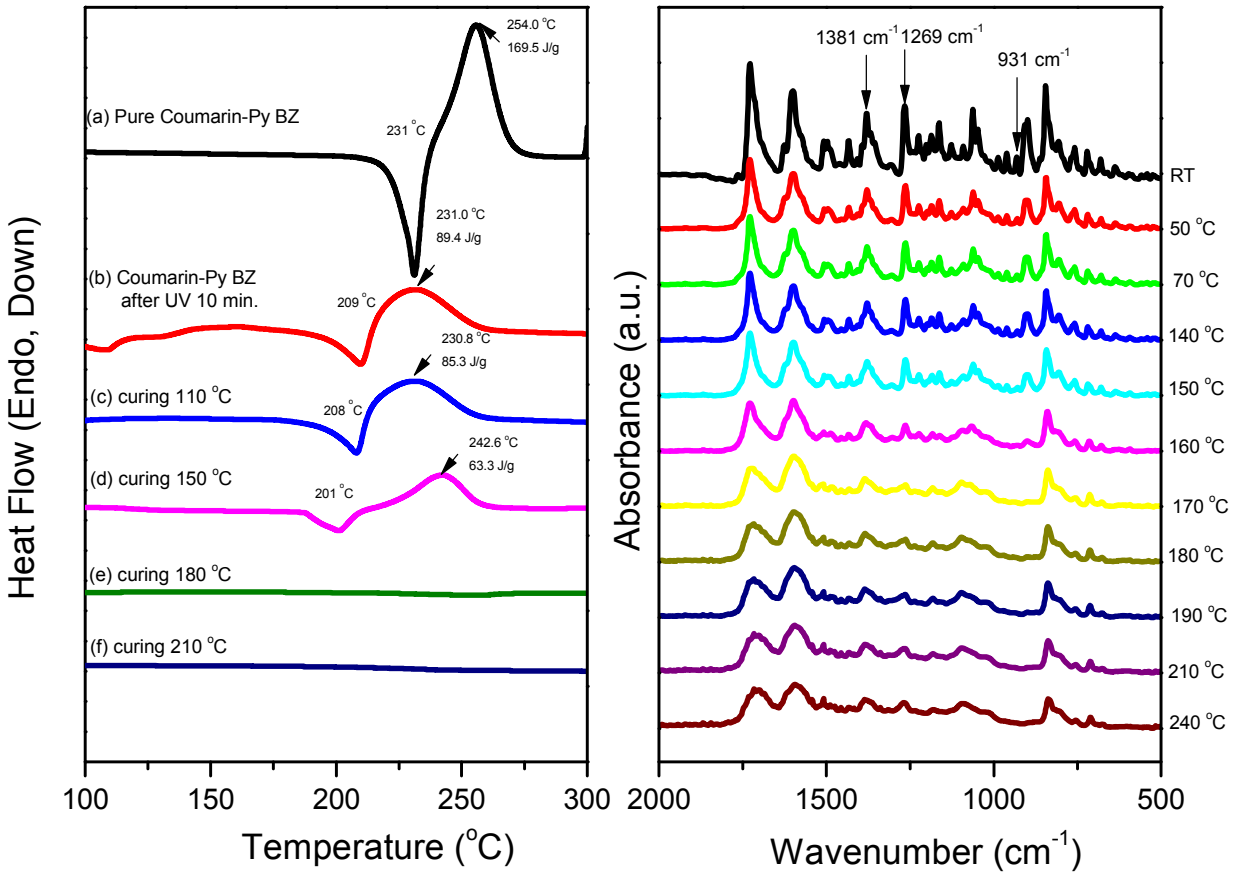

Figure 6: (A) DSC thermograms and (B) FTIR spectra of the Di-Coumarin-PY BZ monomer, recorded after each heating stage.

at 3.7 ppm, was approximately 68%, similar to the value determined using UV–Vis spectroscopy. The ^{13}C NMR spectrum in Figure 5(d) reveals signals at 60.25 and 38.7 ppm for carbon atoms in cyclobutane rings. Thus, the ^{1}H and ^{13}C NMR spectra of Coumarin-Py BZ after UV irradiation are consistent with dimerization of the coumarin moieties as depicted in Scheme 2. We employed DSC and FTIR spectroscopy to investigate the thermal curing behavior of Coumarin-Py BZ after its solution in $CHCl_3$ had been subjected to UV irradiation (forming Di-Coumarin-Py BZ) for 15 min. The DSC trace of uncured Di-Coumarin-Py BZ featured [Figure 6(A)] a broad maximum exothermic peak at 231.0 °C with a reaction heat of 89.4 J g^{-1}, and a melting point at 209.0 °C. The intensity of the exotherms decreased upon increasing the number of heat curing stages, with

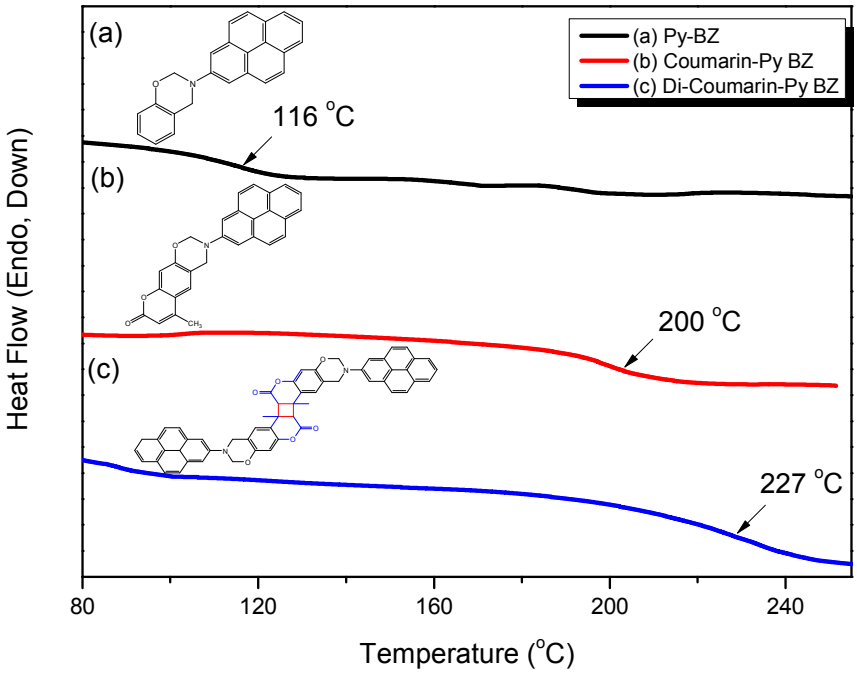

Figure 7: DSC analyses of (a) poly(Py-BZ), (b) poly(Coumarin-Py BZ), and (c) poly(Di-Coumarin-Py BZ), after thermal curing.

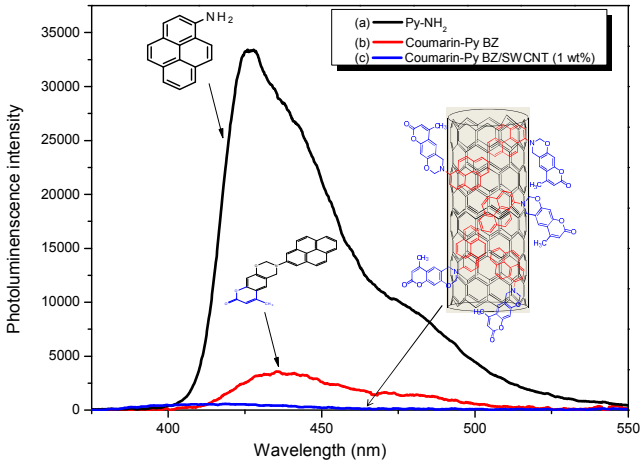

Figure 8: PL spectra of (a) Py-NH_2, (b) Coumarin-Py BZ, and (c) Coumarin-Py BZ/SWCNT (1 wt%).

the exothermic peak disappearing completely after treatment at 180.0 °C; it was significantly lower than that of the pure Coumarin-Py BZ after treatment at 240.0 °C. In addition, we observed that, after dimerization, the maximum exothermic peak and reaction heat were lower than those of the uncured Coumarin-Py BZ (ca. 23 °C and 75 J g^{-1}, respectively). We suggest two possible explanations for these phenomena: (i) dimerization of the coumarin moiety had already occurred, thereby decreasing the reaction heat; (ii) the steric bulk and instability of the cyclobutane ring after dimerization decreased the curing temperature; (iii) the possible destruction of the surface of benzoxazine monomer during irradiation at 365 nm.[26] Figure 6(B) presents the FTIR spectra of the Di-Coumarin-Py BZ monomer and treatment at each curing temperature. All the characteristic absorptions bands of the benzoxazine ring decreased in intensity upon increasing the curing temperature. Interestingly, when the temperature reached 170 °C, these characteristic absorption bands had all disappeared completely; this temperature is also significantly lower than that of pure Coumarin-Py BZ (240.0 °C). This finding is consistent with our DSC results in Figure 6(A). Together, DSC and FTIR spectroscopy suggested that photoinduced crosslinking of coumarin groups acted as a catalyst to accelerate the ring opening of the benzoxazine units.

The backbone rigidity, molecular weight, and crosslinking density of a polymer will affect its glass transition temperature. Figure 7 presents the glass transition temperatures of Py-BZ, Coumarin-Py BZ, and Di-Coumarin-Py BZ after thermal curing. Introduction of a coumarin moiety resulted in Coumarin-Py BZ having a higher value of T_g (200 °C) than that of Py-BZ (116 °C), presumably because of increases in the bulk and the degree of conjugation of the coumarin ring. In addition, the glass transition temperature of Di-Coumarin-Py BZ (227 °C) was much higher than that of pure Coumarin-Py BZ, presumably because the increased crosslinking density after photodimerization of the coumarin moieties limited the mobility of the polymer chains. Figure S4 reveals the thermal stabilities of the Coumarin-Py BZ monomer, poly(Coumarin-Py BZ), and poly(Di-Coumarin-Py BZ) under N_2 atmosphere, as investigated through TGA. The thermal decomposition and char yield of the Coumarin-Py BZ monomer both increased after thermal curing to form poly(Coumarin-Py BZ). In addition, the char yield of poly(Coumarin-Py BZ) increased further after UV irradiation to form poly(Di-Coumarin-Py BZ), again due to the increased crosslinking density after photodimerization of the coumarin moieties. In contrast, the initial thermal decomposition temperature decreased, presumably as a result of destruction of the surface during the UV irradiation process.[26]

The Preparation and Thermal Properties of Coumarin-Py BZ/SWCNT Nanocomposites

Figure 8 displays the PL spectra (excitation at 343 nm) of Py-NH_2, Coumarin-Py BZ, and Coumarin-Py BZ/SWCNT (1 wt%) nanocomposites in THF after curing. The spectrum of Py-NH_2 features a strong fluorescence signal for the pyrene unit at 426 nm; the spectrum of Coumarin-Py BZ features a broad fluorescence signal at 435 nm. In contrast, the spectrum of the

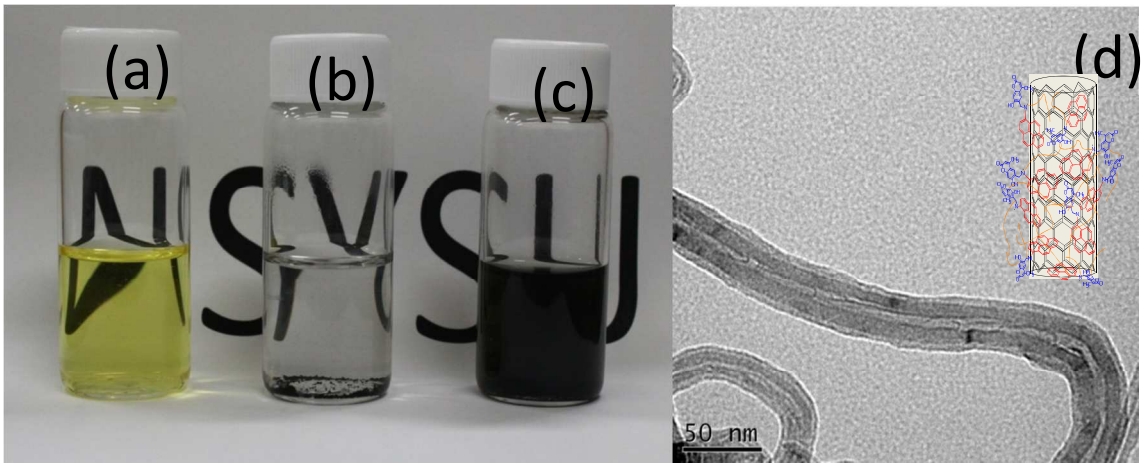

Figure 9: (a–c) Photographs of (a) pure Coumarin-Py BZ, (b) pristine SWCNTs, and (c) Coumarin-Py BZ/SWCNTs (3 wt%) in THF. (d) TEM image of sample (c) after thermal curing.

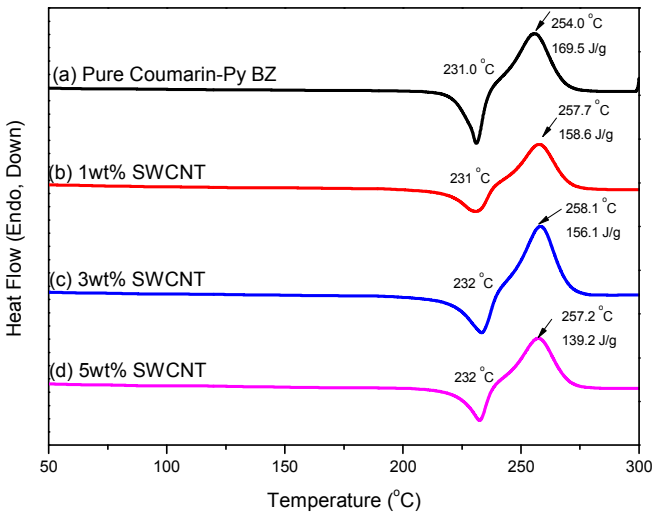

Figure 10: DSC analysis of the un-curing behavior of CoumarinPy BZ mixtures containing various SWCNT contents.

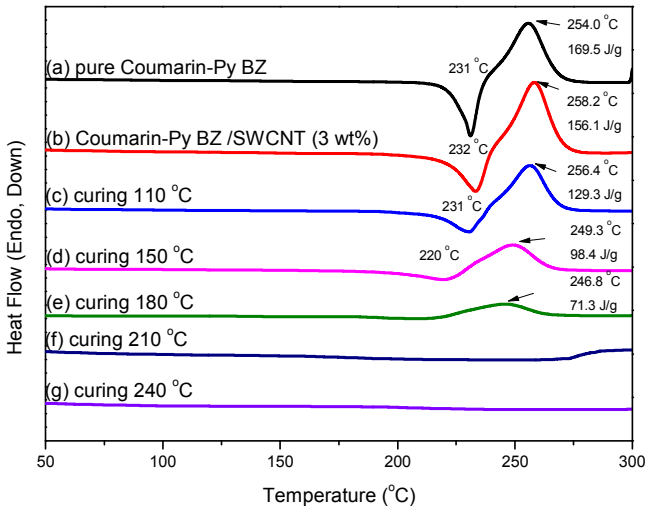

Figure 11: DSC analysis of the curing behavior of the Coumarin-Py BZ/SWCNT (3 wt%) hybrid complex.

Coumarin-Py BZ/SWCNT (1 wt%) nanocomposite features a very weak emission and almost completely quenched fluorescence of the pyrene monomer, suggesting strong π–π stacking interactions between the pyrene moieties of Coumarin-Py BZ and the SWCNTs.[29] Figure 9 displays photographs of THF solutions of Coumarin-Py BZ, pure SWNCTs, and Coumarin-Py BZ in the presence of SWCNTs. The pure Coumarin-Py BZ formed a clear solution [Figure 9(a)], whereas the pure SWCNTs precipitated completely [Figure 9(b)]; the addition of Coumarin-Py BZ into the suspension of the SWCNTs resulted in a dispersion [Figure 9(c)], consistent with soluble complexes having formed as a result of noncovalent interactions (e.g., π-stacking). We used TEM to examine the dispersion of SWCNTs (1 wt%) in the Coumarin-Py BZ matrix. Figure 9(d) reveals a homogenous dispersion of the SWCNTs (black tubes) on the nanoscale. The tubes existed as single entities and were less entangled, without any agglomeration.

Figure 10 presents DSC traces of pure Coumarin-Py BZ and the Coumarin-Py BZ/SWCNT nanocomposites. The curing temperature increased slightly, while the amount of exotherms decreased significantly, upon increasing the SWCNT content. For example, the amount of exotherms after blending 5 wt% of

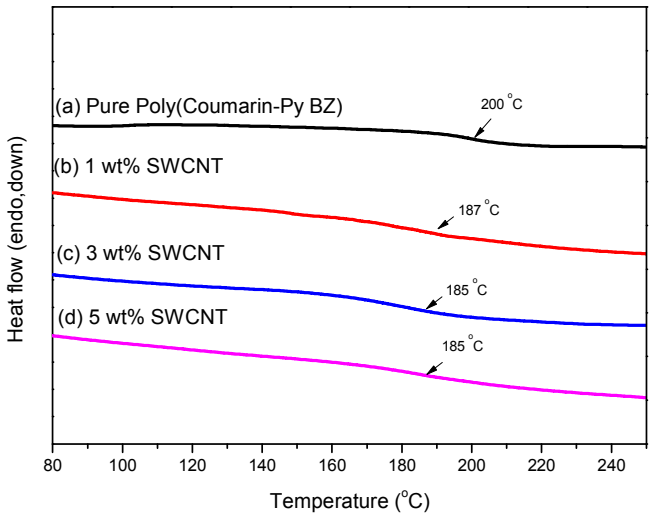

Figure 12: DSC profiles of poly(Coumarin-Py BZ) incorporating various SWCNT contents, after thermal curing.

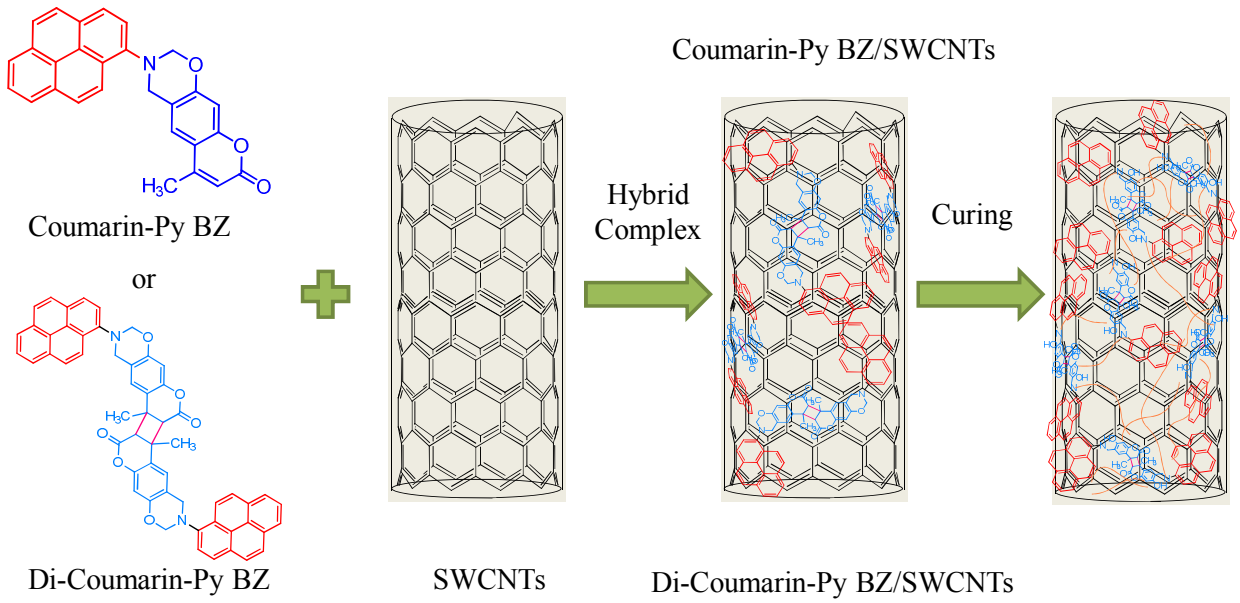

Scheme 3: Preparation of poly(Coumarin-Py BZ)/SWCNT and poly(Di-Coumarin-Py BZ)/SWCNT nanocomposites

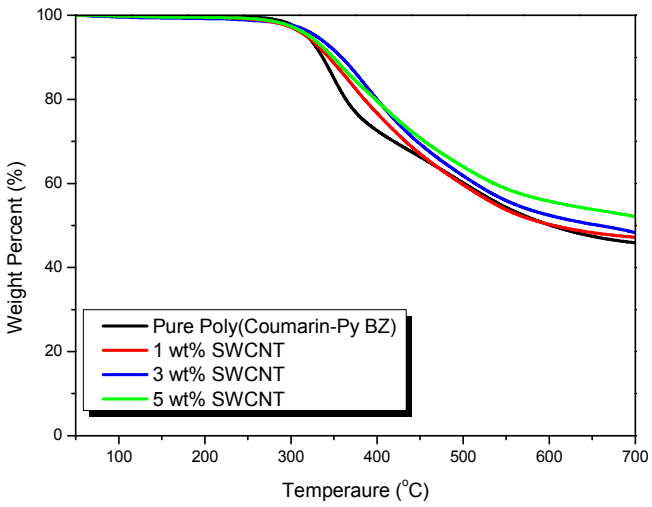

Figure 13: TGA analyses of Coumarin-Py BZ and its mixtures incorporating various SWCNT contents.

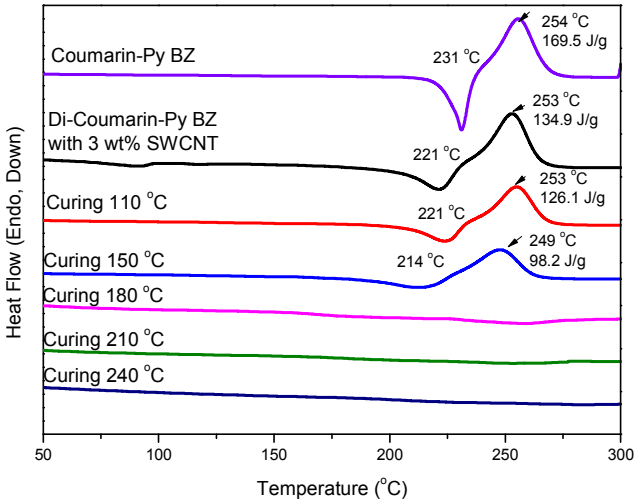

Figure 14: DSC plots of (Di-Coumarin-Py BZ)/SWCNT (3 wt%), after thermal curing.

SWCNTs into Coumarin-Py BZ was 139.2 J g^{-1}, approximately 30.3 J g^{-1} lower than that of pure Coumarin-Py BZ. Kim et al. observed a decrease in the enthalpy of a PBZ derivative after blending with CNTs, attributable to the hindered mobility of the ring-opened benzoxazine, thereby decreasing the crosslinking density of the PBZ.[30] Figure 11 presents the DSC profiles of pure Coumarin-Py BZ and its blend with 3 wt% of SWCNTs, after each curing stage. Again, the amount of exotherms decreased upon increasing the curing temperature, as noted above. A temperature of 240 °C was required for the maximum exothermic peak to disappear completely, similar to that of pure Coumarin-Py BZ in the absence of SWCNTs. Figure 12 displays the effect of the SWCNT content on the glass transition temperature of poly(Coumarin-Py BZ). When the SWCNTs content was 1, 3, or 5 wt%, the glass transition temperature of the nanocomposite was lower (ca. 185–187 °C) than that of pure Coumarin-Py BZ (200 °C). We attribute these lower glass transition temperatures to the lower crosslinking densities of poly(Coumarin-Py BZ) after blending with the SWCNTs. Figure 13 presents the thermal stabilities of these systems under N_2 atmosphere, as investigated using TGA. We used the weight loss temperature (T_{d10}) as the standard. The weight loss temperatures corresponding to the Mannich cleavage of the poly(Coumarin-Py BZ)/SWNCT nanocomposites increased at SWCNT contents of 1 and 3 wt%, but decreased slightly at a SWCNT content of 5 wt%; nevertheless, these values are all higher than that of the pure poly(Coumarin-Py BZ) by approximately 15–30 °C. The relatively higher value for the sample containing 5 wt% SWCNTs suggests a relatively lower degree of thermal decomposition, presumably because of its higher degree of aggregation. We observed that the char yield increased upon increasing of SWCNT content, as expected because the incorporation of SWCNTs would block the premature evaporation of the decomposed molecular fragments, and because of the formation of network structures after introduction of nanohybrid CNTs.[21]

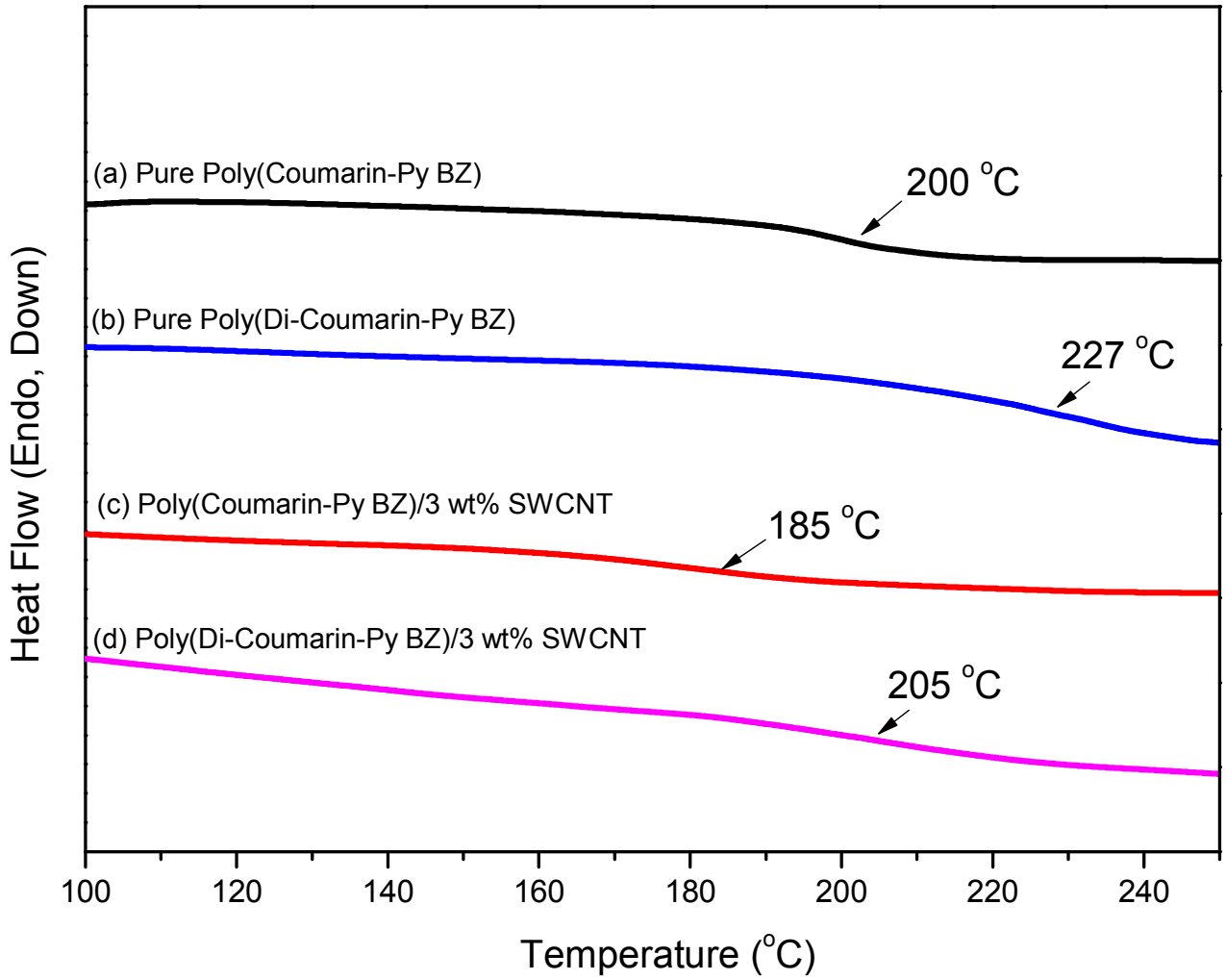

Figure 15: DSC profiles of poly(Coumarin-Py BZ), poly(Di-Coumarin-Py BZ), poly(Coumarin-Py BZ)/SWCNT (3 wt%), and poly(Di-Coumarin-Py BZ)/SWCNT (3 wt%).

Thermal Properties of Di-Coumarin-Py BZ/SWCNT Nanocomposites

As mentioned above, the glass transition temperature (227 °C) and char yield (46.9 wt%) of poly(Di-Coumarin-Py BZ) were much higher than those of pure poly(Coumarin-Py BZ) (200 °C and 44.4 wt%, respectively), due to the increased crosslinking after photodimerization. Nevertheless, the initial thermal decomposition temperature decreased as a result of possible destruction on the surface during irradiation. In contrast, the glass transition temperatures of the poly(Coumarin-Py BZ)/SWCNT nanocomposites were lower than that of pure poly(Coumarin-Py BZ) because of the decreased crosslinking density of poly(Coumarin-Py BZ) after blending with the SWCNTs. The thermal decomposition temperature and char yield increased, however, after blending the SWCNTs into poly(Coumarin-Py BZ), due to blocking of the premature evaporation of the decomposed molecular fragments at the surface of poly(Coumarin-Py BZ). As a result, combining the photo-crosslinkable coumarin groups (high crosslinking density) with a dispersion of SWCNTs (high decomposition temperature) in a PBZ matrix minimized the premature evaporation of the decomposed molecular fragments at the surface (Scheme 3).

Figure 14 displays the DSC profiles for the thermal curing of Coumarin-Py BZ/SWCNT (3 wt%) after UV irradiation for 10 min. The DSC plot of the uncured Di-Coumarin-Py BZ/SWCNT (3 wt%) featured a broad melting point at 221 °C, an exotherm peak having a maximum at 253 °C, with an amount of exotherm of 139.9 J g^{-1}; these values are all lower than those of pure Coumarin-Py BZ, but are all higher than those of uncured Di-Coumarin-Py BZ in the absence of CNTs. Furthermore, the reaction heat of the exothermic peak decreased upon increasing the curing temperature, almost disappearing after curing at 180 °C—the same temperature as that for the pure Di-Coumarin-Py BZ in the absence of CNTs. Figure 15 summarizes the glass transition temperatures of pure poly(Coumarin-Py BZ), pure poly(Di-coumarin-Py BZ), poly(Coumarin-Py BZ)/SWCNT (3 wt%), and poly(Di-coumarin-Py BZ)/SWCNT (3 wt%). The glass transition temperature of pure poly(Di-coumarin-Py BZ) was higher than that of pure poly(Coumarin-Py BZ), due to the higher crosslinking density, but the glass transition temperature of poly(Coumarin-Py BZ)/SWCNT (3 wt%) was lower than that of pure poly(Coumarin-Py BZ), due to the lower crosslinking density. Interestingly, when combining both effects, the glass transition temperature (205 °C) of poly(Di-coumarin-Py BZ)/SWCNT (3 wt%) was still higher than that (200 °C) of pure poly(Coumarin-Py BZ); thus, the increase in the crosslinking density after photodimerization of the coumarin moieties dominated the glass transition behavior in this case. Figure 16 summarizes the TGA data for the Coumarin-Py BZ monomer, poly(Coumarin-Py BZ), poly(Di-Coumarin-Py BZ),

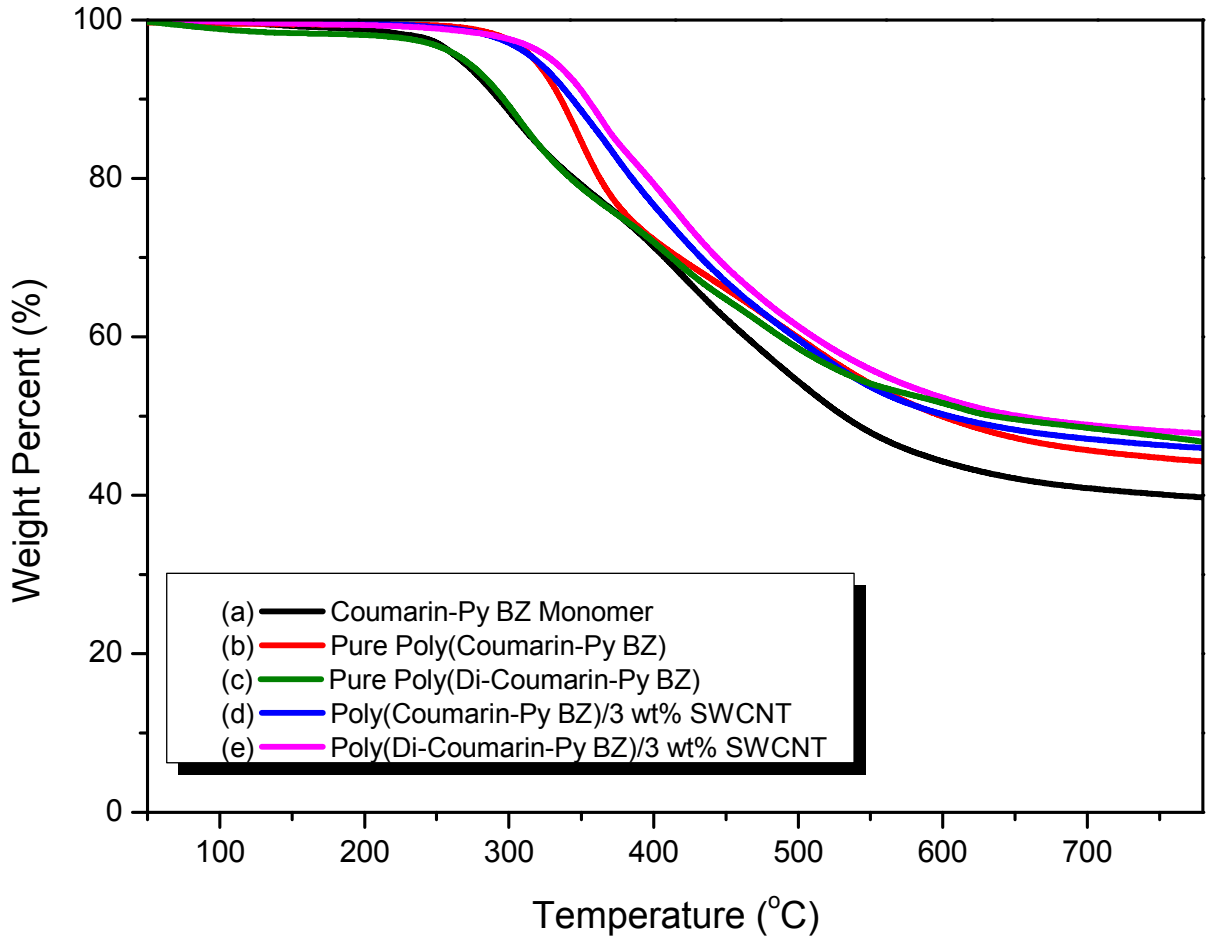

Figure 16: TGA analyses of (a) Coumarin-Py BZ monomer, (b) poly(Coumarin-Py BZ), (c) poly(Di-Coumarin-Py BZ), (d) poly(Coumarin-Py BZ)/SWCNT (3 wt%), and (e) poly(Di-Coumarin-Py BZ)/SWCNT (3 wt%).

poly(Coumarin-Py BZ)/SWCNT (3 wt%), and poly(Di-Coumarin-Py BZ)/SWCNT (3 wt%). Among these systems, the thermal stability of poly(Di-Coumarin-Py BZ)/SWCNT (3 wt%) was the greatest, represented by the highest values of its thermal decomposition temperature (355 °C) and char yield (49 wt%), consistent with the increased crosslinking density after UV irradiation and the nano-reinforcement effect of the CNTs.

Conclusion

We have prepared a new bifunctional benzoxazine monomer containing both coumarin and pyrene moieties. The presence of the coumarin groups (photo-crosslinkable) and pyrene groups (capable of π-stacking with SWCNTs) in the PBZ matrix had several effects: a relatively low thermal curing temperature (180 °C); a high glass transition temperature (205 °C) relative to those of pure poly(Coumarin-Py BZ) (200 °C) and poly(Coumarin-Py BZ) incorporating 3 wt% SWCNT (185 °C); and a high thermal decomposition temperature (355 °C) and char yield (49 wt%). Although poly(Di-Coumarin-Py BZ) displayed a high glass transition temperature, it had a relatively low thermal decomposition temperature because of premature evaporation of decomposed molecular fragments at its surface. Incorporation into SWCNTs inhibited such premature evaporation at the surface, presumably because the inorganic hydrophobic SWCNTs migrated to the surface, thereby enhancing the thermal decomposition temperature. As a result, combining photo-crosslinkable coumarin and pyrene groups into the benzoxazine monomer had considerable effect on its thermal stability. This approach appears to be a good candidate for the preparation of high-performance PBZs.

Acknowledgment

This study was supported financially by the Ministry of Science and Technology, Taiwan, Republic of China, under contracts MOST103-2221-E-110-079-MY3 and MOST102-2221-E-110-008-MY3. We thank Mr. Hsien-Tsan Lin and Mr. Shih-Hung Huang of the Regional Instruments Center at National Sun Yat-Sen University for help with the TEM experiments.

Supporting Information

Electronic supplementary information (ESI) available: Characterization of ^{1}H, and ^{13}C NMR of Py-NH_2, DSC and TGA analyses includes Py-BZ, Coumarin-Py BZ, poly(Coumarin-Py BZ), and poly(Di-Coumarin-Py BZ).

Reference

1 N. N. Ghosh, B. Kiskan, and Y. Yagci, *Prog. Polym. Sci.,* 2007, **32**, 1344-1391.
2 G. Lligads, A. Tuzun, J. C. Ronda, M. Galis, and V. Cadiz, *Polym. Chem.,* 2014, **5**, 6636-6644.
3 X. Li, Y. Xia, W. Xu, Q. Ran, and Y. Gu, *Polym. Chem.*,

2012, 3, 1629-1633.
4 Y. Yagci, B. Kiskan, and N. N. Ghosh, *J. Polym. Sci. Part A: Polym. Chem.,* 2009, **47**, 5565-5576.
5 C. F. Wang, Y. C. Su, S. W. Kuo, C. F. Huang, Y. C. Sheen, and F. C. Chang, *Angew. Chem. Int. Ed.,* 2006, **45**, 2248-2251.
6 S. W. Kuo, Y. C. Wu, C. F. Wang, and K. U. Jeong, *J. Phys. Chem. C.,* 2009, **113**, 20666-20673.
7 C. F. Wang, S. F. Chiou, F. H. Ko, J. K. Chen, C. T. Chou, C. F. Huang, S. W. Kuo, and F. C. Chang, *Langmuir,* 2007, **23**, 5868-5871.
8 C. F. Wang, F. C. Chang, and S. W. Kuo "*Handbook of Polybenzoxazine*", H. Ishida, T. Agag Eds., Elsevier, Amsterdam 2011, *Chapter 33*, 579.
9 Q. Li, and X. Zhong, *Langmuir,* 2011, **27**, 8365-8369.
10 W. H. Hu, K. W. Huang, S. W. Kuo, *Polym. Chem.,* 2012, **3**, 1546-1554.
11 Y. X. Wang, and H. Ishida, *Polymer,* 1999, **40**, 4563-4570.
12 A. Sudo, R. Kudo, H. Nakayama, K. Arima, and T. Endo, *Macromolecules,* 2008, **41**, 9030-9034.
13 H. Ishida "*Handbook of Polybenzoxazine*", H. Ishida, and T. Agag Eds., Elsevier, Amsterdam 2011, *Chapter 1*, 1.
14 H. M. Qi, G. Y. Pan, and Q. Y. Zhuang, *Polym. Eng. Sci*., 2010, **50**, 1751-1757.
15 C. Sawaryan, K. Landfester, and A. Taden, *Macromolecules,* 2010, **43**, 8933-8941.
16 (a) A. Chernykh, T. Agag, and H. Ishida, *Polymer,* 2009, **50**, 3153-3157. (b) T. Agag, and T. Takeichi, *Macromolecules,* 2001, **34**, 7257-7263. (c) T. Agag, and T. Takeichi *Macromolecules,* 2003, **36**, 6010-6017. (d) B. Kiskan, and Y. Yagci, *Polymer,* 2008, **49**, 2455-2460. (e) B. Kiskan, B. Aydogan, and Y. Yagci, *J. Polym. Sci., Part A: Polym. Chem.,* 2009, **47**, 804-811. (f) A. Chernykh, T. Agag, and H. Ishida, *Macromolecules,* 2009, **42**, 5121-5127. (g) S. W. Kuo, and W. C. Liu, *J. Appl. Polym. Sci.,* 2010, **117**, 3121-3127.
17 Y. C. Su, S. W. Kuo, Xu, H. Y. Xu, and F. C. Chang, *Polymer,* 2003, **44**, 2187-2191.
18 (a) T. Agag, and T. Takeichi, *Polymer,* 2000, **41**, 7083-7090. (b) P. Phirivawirut, R. Magaraphan, and H. Ishida, *Mater. Res. Innova.,* 2001, **4**, 187-196. (c) H. K. Fu, C. F. Huang, S. W. Kuo, H. C. Lin, D. R. Yei, and F. C. Chang, *Macromol. Rapid Commun.,* 2008, **29**, 1216-1220. (d) Cui, H. W. Cui, and S. W. Kuo, *Appl. Clay Sci.,* 2014, **91-92**, 1-5.
19 (a) J. Zhang, R. Xu, and D. Yu, *Euro. Polym. J.,* 2007, **43**, 743-752. (b) Q. Chen, R. Xu, J. Zhang, D. Yu, *Macromol. Rapid Commun.,* 2005, **26**, 1878-1882. (c) Y. Liu, and S. Zheng, *J. Polym. Sci., Part A: Polym. Chem.,* 2006, **44**, 1168-1181. (d) Y. C. Wu, and S. W. Kuo, *Polymer,* 2010, **51**, 3948-3955. (e) K. W. Huang, and S. W. Kuo, *Macromol. Chem. Phys.,* 2010, **211**, 2301-2311. (f) S. W. Kuo, and F. C. Chang, *Prog. Polym. Sci.,* 2011, **36**, 1649-1696. (g) W. H. Hu, K. W. Huang, C. W. Chiou, and S. W. Kuo, *Macromolecules,* 2012, **45**, 9020-9028.
20 (a) C. H. Frey, *Polymer,* 2013, **54**, 5443-5455, (b) P. D. Petrov, G. L. Georgiev, and A. H. E. Muller, *Polymer,* 2012, **53**, 5502-5506. (c) Y. Y. Liang, J. Z. Xu, X. Y. Liu, G. J. Zhong, Z. M. Li, *Polymer,* 2013, **54**, 6479-6488. (d) Q. Chen, R. Xu, and D. Yu, *Polymer,* 2006, **47**, 7711-7719. (e) C. M. Chang, and Y. L. Liu, *ACS Appl. Mater. Interfaces,* 2011, **3**, 2204-2208. (f) M. Chapartegui, J. Barcena, X. Irastorza, C. Elizetxea, M. Fernandez, and A. Santamaria, *Comp. Sci. Tech.,* 2012, **72**, 489-497. (g) L. Dumas, L. Bonnaud, M. Olivier, and P. Dubois, *Chem. Commun.,* 2013, **49,** 9543-9545.
21 C. C. Yang, C. Y. Lin, Wang, I. Po. Wang, J. D. Liaw, and W. S. Kuo, *Polymer,* 2014, **55**, 2044-2050.
22 (a) G. B. Xing, W. C. Yu, H. K. Chow, L. P. Ho, G. D. Fu, and B. Xu, *J. Am. Chem. Soc*., 2002, **124**, 14846-14847. (b) K. J. Klosterman, Y. Yamauchi, and M. Fujita, *Chem. Soc. Rev*., 2009, **38**, 1714-1725. (c) S. Lena, S. Masiero, S. Pieraccini, and P. G. Spada, *Chem. Eur. J*., 2009, **15**, 7792-7806.
23 (a) Q. Cao, and J. A. Rogers, *Adv. Mater*., 2009, **21**, 29-53. (b) S. M. Bachilo, M. S. Strano, C. Kitterll, R. H. Hauge, R. E. Smalley, and K. B. Weisman, *Science,* 2002, **298**, 2361-2366.
24 Y. Huang, R. Dong, X. Zhu, and D. Yan, *Soft Matter,* 2014, **10**, 6121-6138.
25 (a) J. Babin, M. Lepage, and Y. Zhao, *Macromolecules,* 2008, **41**, 1246-1253.(b) J. Jiang, B. Qi, M. Lepage, and Y. Zhao, *Macromolecules,* 2007, **40**, 790-792.
26 Yagci, Y.; Kiskan, B. *J. Polym. Sci.; Part A: Polym. Chem*., **2007**, 45, 1670-1676.
27 H. Ishida, "*Handbook of Polybenzoxazine*", H. Ishida, and T. Agag, Eds., Elsevier, Amsterdam 2011, *Chapter 1*, 1.
28 (a) A. T. Moore, L. M. Harter, and S. P. Song, *J. Mol. Spectroscopy.,* 1971, **40**, 144-157. (b) D. Kehrloesser, J. Traegar, C. H. Kim, and N. Hampp, *Langmuir,* 2010, **26**, 3878-3882.
29 (a) C. M. Chang, and Y. L. Liu, ACS Appl. Mater. Interfaces, 2011, 3, 2204-2208. (b) M. Chapartegui, J. Barcena, X. Irastorza, C. Elizetxea, M. Fernandez, and A. Santamaria, Comp. Sci. Tech. 2012, 72, 489-497.
30 K. Kaleemullah, S. U. Khan, and J. K. Kim, *Comp. Sci. Tech.,* 2012, **72**, 1968-1976.

A Graphic Content

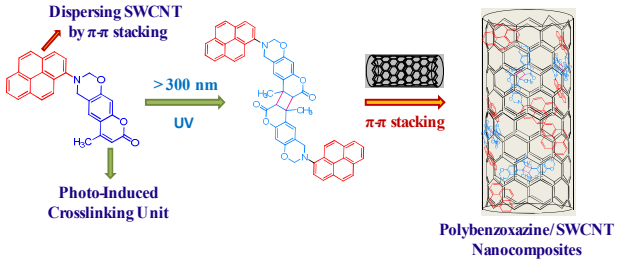

A new bifunctional benzoxazine monomer possessing both coumarin and pyrene groups for photo-crosslinking and dispersing for single-walled carbon nanotubes.